PCCP

Accepted Manuscript

ROYAL SOCIETY OF CHEMISTRY

www.rsc.org/pccp

A multilayered-representation, quantum mechanical/molecular mechanics study of the CH$_3$Cl + F$^-$ reaction in aqueous solution: reaction mechanism, solvent effects and potential of mean force

Jingxue Zhang[†], Yulong Xu[†‡], Jie Chen[†], Dunyou Wang[†]*

[†]College of Physics and Electronics, Shandong Normal University, Jinan, 250014 China

[‡]School of Science, Qilu University of Technology, Jinan, 250353 China

[*]Corresponding Author : dywang@sdnu.edu.cn

ABSTRACT

A multilayered-representation, quantum mechanical and molecular mechanics approach was employed to study the bimolecular nucleophilic substitution reaction of $CH_3Cl + F^-$ in aqueous solution. The affected reactant complex, transition state and product complex, in the presence of the aqueous solution, were analyzed along the reaction pathway. A multilayered representation which includes the density function theory and coupled-cluster single double (triple) (CCSD(T)) theories for the reaction region was used to compute the potentials of mean force for this reaction in aqueous solution. The obtained free energy activation barrier at the CCSD(T)/MM representation is 23.2 kcal/mol, which agrees well with the experimental value at 26.9 kcal/mol. The calculated reaction free energy, -8.0 kcal/mol, has an excellent agreement with the estimated value, -8.1 kcal/mol, in solution obtained based on the solvation energies and reaction energy from gas phase. The solvation energy raises the activation barrier by 17.0 kcal/mol, while the polarization effect only raises the activation barrier by 1.5 kcal/mol. All in all, the aqueous solution plays an essential role in shaping the reaction pathway for this reaction in water.

I. INTRODUCTION

The wide use of halogenated hydrocarbons in industry and agriculture, such as electrical insulators, pesticides and organic synthesis etc., makes halogenated hydrocarbons a serious pollution source of the surface/ground water and atmosphere.[1,2] Most of the halogenated hydrocarbon are persistent in the environment; thus widespread human exposure occurs in both nature and working environment. The accumulation of these chemicals in organisms can cause toxicity or even cancer so that many halogenated hydrocarbons are included in the 126 priority pollutants listed by the US environmental protection agency.[3] Since halogenated hydrocarbons are major pollutants not only in atmosphere but also in soil, surface and ground water, it's important to study the reactions of the halogenated hydrocarbons in both gas-phase and aquatic environment.

For the bimolecular nucleophilic substitution(S_N2) CH_3Cl+F^- reaction in gas-phase, Bohme's group[4,5] measured the rate constants of the F^- anion reaction with CH_3Cl,[4] and the influence of stepwise solvation on the nucleophilicity of F^- using the flowing afterglow technique.[5] Researchers from Hase's group[6] performed the trajectory and kinetics studies on the CH_3Cl+F^- reaction in gas phase. Hu and Trublar[7] did the electronic structure calculation to determine the reactant, product and saddle point of $CH_3Cl+F^-(H_2O)$ in gas phase. Igarashi and Tachikawa studied the potential energy surface and carried out direct dynamics calculation on the CH_3Cl+F^- in gas phase,[8,9] as well as on the micro-solvated reaction of $CH_3Cl+F^-(H_2O)$.[10-12] Recently, a quasiclassical trajectory study for the CH_3Cl+F^- in gas phase using a new full-dimensional ab-initio potential energy surface has also been reported.[13] In aqueous solution, Bathgate and Moelwyn-Hughes[14] measured the reaction rates and derived that the activation barrier is 26.9 kcal/mol for the title reaction; Kozaki et al.,[15] by

introducing the solvent dielectric constant into the MNDO Fock matrix, found that the potential energy curve of CH_3Cl+F^- changes from double-well type to the unimodal type when dielectric constant of the solvent increases with the MNDO-effective charge model.

So far, there have been no quantitative, accurate free energy profile reported for the CH_3Cl+F^- reaction in solution with an explicit water environment, not to mention the accurate solvent effects' contribution to the energetic along the free energy reaction profile. So, in this study, we want to explore the solvent-influenced geometries of the reactant, transition state and product state for this reaction in aqueous phase, to investigate the evolution of the structures and charges along reaction pathway, to not only get a quantitative picture of the reaction pathway but also calculate the potential of mean force (PMF) with the reaction region described by the high accuracy CCSD(T) level of theory, as well as the accurate solution contribution to the PMF.

For reactions in aqueous solution, the water environment inevitably brings a tremendous number of degrees-of-freedom into the reaction system; therefore, direct quantum mechanical calculation on the whole system is impractical. Here we employed the combined quantum mechanical and molecular mechanics (QM/MM) approach to simulate the reaction mechanism,[16-18] applying quantum mechanical (QM) description to the reactive solute region and molecular mechanics (MM) level theory to the rest of the system. However, even with this simplified approach, the free energy computation still remains a formidable challenge. As a result, the QM region is typically treated with density functional theory (DFT),[19,20] which usually introduces a sizable uncertainty in description of the reaction energetics, especially for the transition state energy barrier.[21] Therefore, we employ a multilayered representation to describe the QM region with electrostatic potential(ESP), DFT and CCSD(T)[22,23]

4

level theories at different stages of the computation. By doing so, we can shift the burden of statistical sampling of the solvent to the less expensive and more efficient ESP and DFT representations, and at the final stage of the computation, then shift back to a much more accurate CCSD(T) representation to obtain the high accurate PMF. In this work, the S_N2 reaction $CH_3Cl + F^- \rightarrow CH_3F + Cl^-$ in water solution was investigated using the multilayered-representation, QM/MM method.[24-26] In our QM/MM calculation, all the solvation water molecules are treated explicitly using the molecular mechanics approach. The ONIOM method[27] usually incorporates solvent effects via the polarizable continuum model (PCM) to deal with the aqueous environment.[28] The continuum solvation models, such as PCM[29] and COSMO[30] have been proven to be reliable in calculating solvation energies of stationary points; however, their performance for reaction energetics is lesser-known. On mapping the potential of mean force, explicit atomistic description of the aqueous environment may be required.

II. METHODOLOGY

Calculations presented in this work were accomplished using QM/MM capabilities of NWChem computational chemistry package.[31] Under this multilayered-representation, combined QM and MM approach, the reactant $CH_3Cl + F^-$ was treated as the QM region; the water environment, the MM region. The energy of the whole system can be written as,

$$E = E_{qm}(r, \varphi) + E_{mm}(R) + E_{qm/mm}(r, R, \rho) \tag{1}$$

where r, R are the coordinates of the QM and MM regions, respectively; and φ represents the electronic degrees of freedom corresponding to the ground state of the QM region. The first term, E_{qm}, is the solute QM energy with the expression in gas phase; the second term, E_{mm}, contains the classical energy of the solvent, as wells as

5

the van der Waals and the Coulomb nuclear solvent-solute interaction energy; the $E_{qm/mm}$ denotes the electrostatic interactions between the solute electron density ρ and solvent classical charges Z_I, which can be approximated as,[17]

$$\sum_I \int \frac{Z_I \rho(r')}{|R_I - r'|} dr' = \sum_{iI} \frac{Z_I Q_i}{|R_I - r'|} = E_{esp}(r, R, Q) \qquad (2)$$

here the solute electronic density is represented by the electrostatic potential(ESP) charges.

The potential of mean force (PMF) along the reaction pathway in aqueous solution can be calculated as

$$W(r, \beta) = -\frac{1}{\beta} \ln \int e^{-\beta E(r, R; \varphi)} dR \qquad (3)$$

where $\beta = 1/(kT)$.

Because direct computation of the PMF on the $CCSD(T)$[22,23] level of theory is unrealistic, a multilayered-representation, QM/MM method containing CCSD(T)/MM, DFT/MM and ESP/MM were employed here. We started from the low level, relatively inexpensive DFT/MM level of theory, then shifted the calculation to the CCSD(T)/MM level theory to achieve the high accurate PMF. Before shifting to the CC representation, we calculate the DFT energy under the Hartree-Fock exact exchange functional; then based on the above DFT reference orbitals, we compute the CCSD(T) correlation energy under the CC representation; finally, the total CCSD(T) energy is obtained by adding the two parts' energy together. The PMF at the final CCSD(T)/MM level of theory can be written as[24]

$$\Delta W_{A,B}^{CC} = (\Delta W_{A,A}^{CC \rightarrow DFT} - \Delta W_{B,B}^{CC \rightarrow DFT}) + (\Delta W_{A,A}^{DFT \rightarrow ESP} - \Delta W_{B,B}^{DFT \rightarrow ESP}) + \Delta W_{A,B}^{ESP} \qquad (4)$$

here, the first term stands for free energy difference for shifting the representation from DFT to CCSD(T) at the fixed solute configuration (A or B); the second term is

6

the same except for shifting the representation from ESP to DFT. The third term, the

solvent contribution to the PMF, was calculated using finite difference

thermodynamics perturbation theory from A to B solute configuration at the classical

ESP/MM representation.[24] Note the last two terms combined is the PMF at the

DFT/MM level of theory.

First, the initial structure of the reactant $CH_3Cl + F^-$ complex, was taken from

previous studies[8] in gas phase, and was solvated in a 34.4 Å cubic box consisting of

1351 water molecules. These water molecules, regarded as the MM region, were

described using SPC/E[32] water model. For the DFT/MM calculation, the B3LYP

exchange correlation functional was applied to deal with the solute QM region, and

the aug-cc-pvDZ basis was used in both DFT and CCSD(T) calculations. Truhlar and

coworkers[33] have assessed several electronic structure methods and basis sets on the

accuracy of the barrier height for several S_N2 reactions in gas phase. Based on their

calculation results, they recommend the basis sets cc-pVTZ+, MG3S, MG3SXP and

aug-cc-pVDZ for the DFT calculations when larger basis sets are affordable.

Therefore, we adopt the aug-cc-pVDZ basis set for the current calculation.

Furthermore, in a study of assessment of DFT for model S_N2 reactions by Gonzales

et. al,[34] they find the hybrid B3LYP functional outperforms the widely employed pure

functionals in reaction energies and particularly the net activation barriers. Therefore,

we adopt the B3LYP functional for the current study. Moreover, from the experience

of our previous studies[24,25,35] on the reactions in solution, the combination of aug-cc-

pVDZ basis and B3LYP gives us reliable reaction energetics along the reaction

7

pathway. Thus in the current study, we still use the combination of the aug-cc-pVDZ basis and B3LYP functional. The van der Waals parameters for the QM region were obtained from the standard Amber force field.[36]

Second, after the setup procedure, the whole system was optimized using the multi-region optimization in NWChem; then the solvent was equilibrated using 40ps molecular dynamics simulation at a temperature of 298 K; meanwhile, the solute region was represented by the ESP charges calculated in the prior optimization step. After the equilibration step, the system was again fully optimized and was used as the original reactant state for all subsequent simulations. Next, the original product complex CH_3F/Cl^- was determined using the original reactant complex through a C-Cl bond breaking and C-F bond forming process. The equilibration and optimization steps again were employed to obtain the optimized initial product complex in water.

Third, based on the above obtained original reactant and product complexes in water, the reaction pathway was searched using the nudged elastic band[37] (NEB) method with 10 replicas, in which the one with highest energy value (NO.5 bead in this case) was used for the saddle point search. The transition state structure was verified through the numerical frequency calculations, which showed one imaginary frequency along the reaction coordinates in water. By optimizing the displacements of the transition state along the imaginary frequency mode, we obtained the final reactant and product complexes to construct the final NEB reaction pathway. Based on the newly found reactant and product complexes, a new 10-point NEB reaction pathway was constructed; to guarantee sufficient relaxation of the solvent, we equilibrated the solvent around the reaction pathway with molecular dynamics simulations for 40ps for each bead, and then optimized the whole NEB reaction

pathway again. This cycle was repeated until the final NEB minimum energy path converged.

Last, the PMFs under the DFT/MM and CCSD(T)/MM representations along the converged reaction pathway were calculated according to Equation 4.

III.   RESULTS AND DISCUSSIONS

A. Reactant complex

The reactant state complex of the reaction $CH_3Cl + F^- \rightarrow CH_3F + Cl^-$ in aqueous phase is presented in Figure 1. Comparing with the gas phase reactant complex,[8] the two biggest differences are the distance from the nucleophile F^- to the C atom in the substrate and the angle $\angle Cl$-C-F formed by the leaving group Cl, the center atom C and the nucleophile F^-. The C-F distance is much longer at 2.65 Å in aqueous solution than that at 2.40 Å in gas phase; the angle of $\angle Cl$-C-F is 180º in gas-phase, while it is 169º in aqueous solution. These two big differences are both caused by the solvation effects. For the first difference, the longer C-F distance in aqueous solution is due to the solvation shielding effect from the water environment: the nucleophile F^- forms seven hydrogen bonds with the surrounding water molecules with an average hydrogen bond distance around ~2.61 Å. In other words, the presence of solution weakens the interaction between CH3Cl and F^-; consequently, the longer C-F distance than that in the gas phase. As for the second difference, the seven hydrogen bonds formed with the F^- nucleophile are unevenly distributed: four are above the F^- atom and three are below the F^- atom, which produces an uneven force to pull the F atom upwards to form the bending Cl-C-F angle at 169º. Thus, the solvent plays a big role in influencing the reactant complex in solution.

B. Transition state

The transition state shown in Figure 2 is the fifth bead on top of the NEB reaction pathway, and is confirmed with an imaginary frequency of $310.5i$ cm^{-1} in aqueous solution. As demonstrated in Figure 2, the three H atoms are going through an inversion process as the three $\angle$H-C-F angles change from 73° at reactant to 86° at transition state concertedly, which almost forms a plane with C atom to be perpendicular to F-C-Cl. One thing especially needs to be pointed out is that the F$^-$ here only accepts five hydrogen bonds with an average length of 2.57 Å. This is expected as the nucleophile gets closer to the substrate at the transition state, the electrostatic interaction between the charged F$^-$ and the polar CH$_3$Cl makes the nucleophile less electronegative than at the reactant state; as a result, the nucleophile F$^-$ now forms less hydrogen bonds than at reactant state. Meanwhile, the F-C distance is lessened to 2.11Å at transition state from 2.65 Å at reactant state, and the C-Cl bond was elongated to 2.37 Å at transition state from 1.84 Å at reactant state. Note these two distances are both longer than those at transition state in gas phase[8] with R_{CF} = 1.997 Å and R_{CCl}=2.106 Å. This effect here, again, is caused by the solvent shielding effects.

C. Product state

The product state shown in Figure 2 is the final bead on the reaction pathway in water. At this stage, the inversion process of the three hydrogen atoms are finished with the three $\angle$H-C-F angles at 107.2° in average. Here, the leaving Cl$^-$ group located at a distance of 3.40 Å from the central carbon atom is detached from the substrate, while the attacking F is bonded to CH$_3$ with a CF bond at 1.46 Å. Note this C-F bond here is still longer than the gas phase value at 1.41 Å. For the product state, the solvent caging effect in aqueous solution plays a critical role on stabilizing the Cl$^-$---CH$_3$F complex, which keeps the leaving group from completely moving away

from the CH_3F; however, this final product does not exist in gas phase. We observe

eight water molecules surround the leaving group Cl^- with the mean bond length at

2.79 Å.

Comparing to the previous study of $CH_3Cl + OH^{-35}$, the distances formed by the

nucleophile OH^- with the center C atom are 3.08 Å at reactant state, 2.29 Å at

transition state, and 1.44 Å at product state, which are longer than $CH_3Cl + F^-$ at

reactant state and transition state at 2.65 Å and 2.11 Å, almost the same at product

state at 1.45 Å. This is not surprising , because F^- is more electronegative than OH^- ,

F^- forms stronger interaction than Cl^- does with the substrate.

D. Evolution along the NEB reaction pathway

Figure 3 and Figure 4 show the reaction mechanism of the $CH_3Cl + F^- \rightarrow CH_3F$ +

Cl^- in water from two aspects: the configuration evolution and the charge distribution

evolution along the NEB reaction pathway. Both evolutions demonstrate a

synchronized S_N2 reaction process. On one hand, Figure 3 shows a synchronized

configuration evolution: As the reaction progresses from the reactant(3.1) to transition

state (3.5) , finally to product (3.10), the F-C distance decreases from 2.65 Å to 2.11

Å , finally to 1.45 Å; at the mean time, the C-Cl distance increases from 1.84 Å to

2.37 Å, finally to 3.40 Å simultaneously. On the other hand, Figure 4 shows a

synchronized charge distribution evolution: At the reactant state, the charge of q(CH3)

and q(Cl) keep the substrate neutral, while the F^- nucleophile has the sole negative

charge -1.0; as the reaction progresses, the nucleophile F^- transfers its negative charge

to the substrate so that the nucleophile and the leaving group almost have the equal

amount of charge at transition state (bead 5) about ~ -0.83. After this dividing point,

the negative charge increases on the leaving group, until it fully possesses the whole

negative charge at the product state while the new formed CH_3F is neutral now.

E. Potential of mean force

Potentials of mean force along the NEB pathway under CCSD(T)/MM and DFT/MM representations are plotted in Figure 5 along with the solution free energy contribution which is the $\Delta W_{A,B}^{ESP}$ term in Equation 6. Here, we calculated the relative free energies along the reaction pathway by taking the reactant (bead 1) as the reference point. The free energy activation barrier in the aqueous phase is 23.2 kcal/mol under CCSD(T)/MM representation, while the DFT/MM representation underestimates the barrier height at 20.1 kcal/mol. Both barrier heights in aqueous phase are much larger than the gas-phase, experimental barrier height at 6.9 kcal/mol.[38] That is, the water solution dominates, actually hinders, the reactivity of this reaction in aqueous solution. Indeed, the solvent energy contribution in this Figure shows that the water solution contributes about 17.0 kcal/mol to the activation barrier for the reaction in solution, also 12.4 kcal/mol to the reaction free energy. This figure also shows that the reaction free energy is -10.9 kcal/mol at DFT/MM level of theory and -8.0 kcal/mol at CCSD(T)/MM level of theory.

The discrepancy of the free energy barrier between the calculated and experimental one comes from two sources: the first is from the intrinsic computation errors in ab initio electronic structure methods (DFT with B3LYP/aug-cc-pVDZ and CCSD(T) with aug-cc-pVDZ basis set) we used in this study. However, we cannot estimate this part of computation errors at this point on the current calculation. The second, which is the main cause of the discrepancy, is from the statistical sampling of the water solution contribution to the PMF (the last term in Equation 4) from the MM part. Indeed, we found the variational computational uncertainty of the sampling ranges from about $\pm 0.02\%$ to $\pm 3.6\%$ (about ± 0.04 kcal/mol to ± 0.8 kcal/mol) for the

ten configurations along the PMF reaction pathway. Thus these two reasons lead to the discrepancy of the free activation barrier between the two results.

In Figure 6, we compare our calculated PMF reaction profile with the estimated schematic PMF in aqueous solution which was obtained based on the gas phase[8,9,38] reaction profile. We know the available solvation energies[39,40] for the reactants and products from the gas phase: CH_3Cl (-2.1 kcal/mol), CH_3F (-2.7 kcal/mol) , Cl^- (-73.89 kcal/mol) and F^- (-100.39 kcal/mol), and also the reaction energy in gas phase (-34.0 kcal/mol[9]). Combining these numbers in gas phase produces a reaction free energy of -8.1 kcal/mol in solution. This information along with the experimental value of the activation barrier of 26.9 kcal/mol[14] in water solution was used to construct the estimated schematic PMF (red line) along the reaction path, which was plotted against our PMF(black line) in Figure 6. This Figure shows that the PMF from this work under the CCSD(T)/MM representation agrees quite well with the estimated PMF in aqueous solution. Our PMF has a reaction free energy of -8.0 kcal/mol which agrees excellently with the estimated PMF one of -8.1 kcal/mol. Our calculated free energy barrier height at 23.2 kcal/mol also has a quite good agreement with the experimental value at 26.9 kcal/mol.

The influence of the aqueous environment on PMF results from two sources: one is the solvation energy, and the other is the polarization effect. We have already seen, from Figure 5, that the solvation energy(black line) has a tremendous role in shaping the PMF by contributing ~17.0 kcal/mol to the transition state barrier height and ~12.4 kcal/mol to product state under the CCSD(T)/MM level of theory. The polarization effect, coming from perturbation to the electronic structure of the QM region by the solvent, can be analyzed by comparing the gas-phase and internal QM/MM energy as shown in Figure 7 with the gas-phase reactant as the energy

13

reference point. Here the gas-phase reaction pathway under the CCSD(T) level of theory was calculated using the same 10 beads on the NEB reaction pathway but without the solvent-solute interaction and the solvent environment contribution. The results indicate that the polarization effect increases the reactant state free energy by 11.4 kcal/mol, transition state by 12.9 kcal/mol and product by 14.1 kcal/mol. As a result, the net contribution of polarization on the barrier height is 1.5 kcal/mol and 2.7 kcal/mol on the reaction free energy. Therefore, the aqueous environment, combining the solvation energy and the polarization effect, raised the transition state barrier height by 18.5 kcal/mol; however, the solvation energy is the dominant player as it provides ~92% of the contribution, while the polarization effect only provides ~ 8% of the contribution. Nonetheless, the aqueous solution plays a significant role in shaping the reaction profile.

   Comparing to the previous study of $CH_3Cl + OH^{-}$[35], for which the combined solvation energy and polarization contribution, raising the reaction barrier height by 22.4 kcal/mol, is bigger than that of the $CH_3Cl + F^-$ raising the barrier by 18.5 kcal/mol. S_N2 reactions are very sensitive to steric effects, and since OH^- nucleophile has a bigger size than F^-, the steric hindrance make OH^- harder to access CH_3Cl than F^- does; more importantly, for the reactant of $CH_3Cl + OH^-$, OH^- is attached to one of the H atom in the substrate, so for OH^- to attack C atom, OH^- has to first rotate itself away from the H atom to the center to face C atom, which makes it much difficult for OH^- to attach C than F^-; however, for the $CH_3Cl + F^-$ reactant, F^- is directly attached to C atom and can attack the center C atom directly. Therefore, the above reasons make $CH_3Cl + OH^-$ a slower reaction than $CH_3Cl + F^-$ in aqueous solution.

14

CONCLUSION

The S_N2 reaction $CH_3Cl + F^- \rightarrow CH_3F + Cl^-$ in aqueous solution was simulated using a hybrid QM/MM approach in this study. In order to achieve high accuracy results on CCSD(T) level of theory with the QM region for the PMF, we employed a multi-layered representations, including ESP/MM, DFT/MM and CCSD(T)/MM representations, to shift the expensive computation of statistical sampling to the relative fast and efficient representations of DFT/MM and ESP/MM. The reactant, product, and transition states, under the presence of the water solution, were determined on the NEB reaction pathway. On one hand, the solvation shielding effect weakens the interaction between the nucleophile and the substrate in the reactant complex; on the other hand, the solvation caging effect keep the final product complex together. The calculated reaction activation barrier under the CCSD(T)/MM representation is 23.2 kcal/mol which agrees well with the experimental value at 26.9 kcal/mol[14] in water; the calculated reaction free energy is -8.0 kcal/mol which agrees excellently with the estimated one obtained based on the gas-phase reaction energy, reactant and product solvation energies. The solvation energy and polarization effect combined increases activation barrier by 18.5 kcal/mol, and increases reaction free energy by 15.1 kcal/mol. The solvent effect plays a dominant role in shaping the PMF.

ACKNOWLEDGMENTS

Reactant Complex of Gas Phase
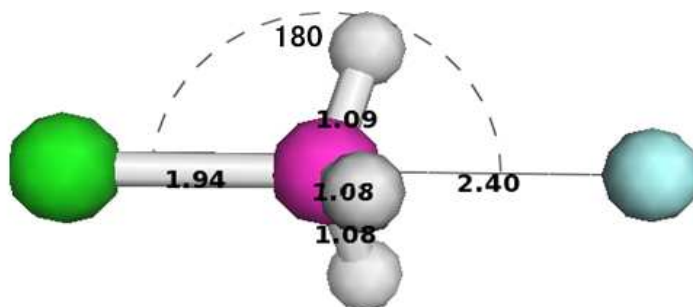
Reactant Complex of Aqueous Solution
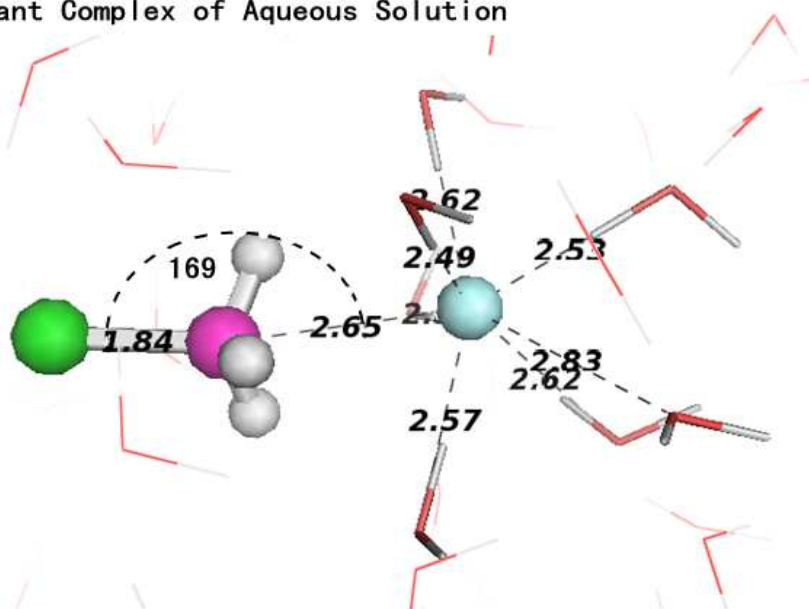
Figure 1. Structures of the reactant complex for the reaction $CH_3Cl + F^- \rightarrow CH_3F + Cl^-$ in gas phase and in aqueous solution. The indicated distances are in Angstroms.
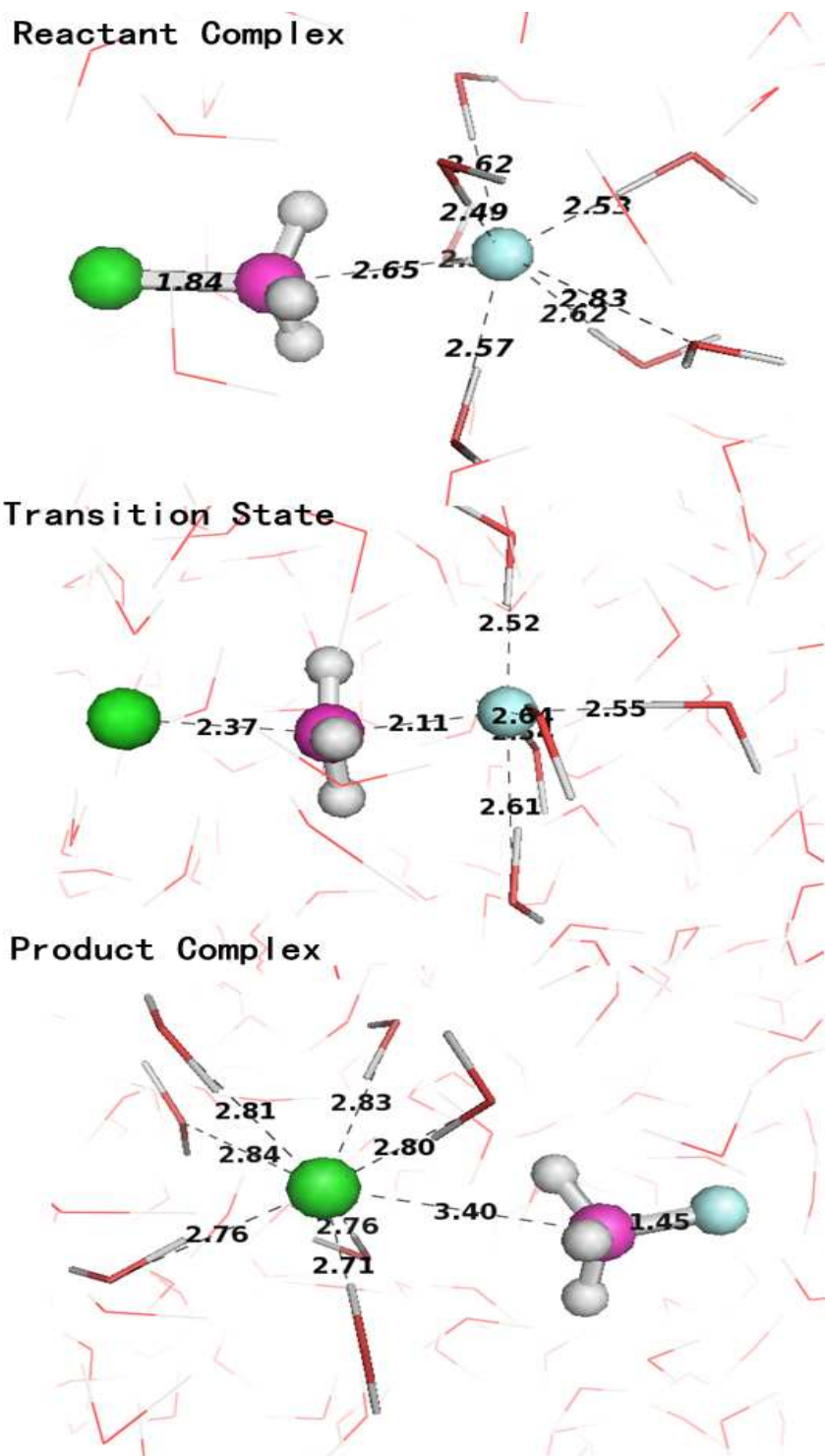
Figure 2. Structures of the reactant complex, transition state, and product complex for

the $CH_3Cl + F^- \rightarrow CH_3F + Cl^-$ reaction in aqueous phase. The indicated distances are

in Angstroms.
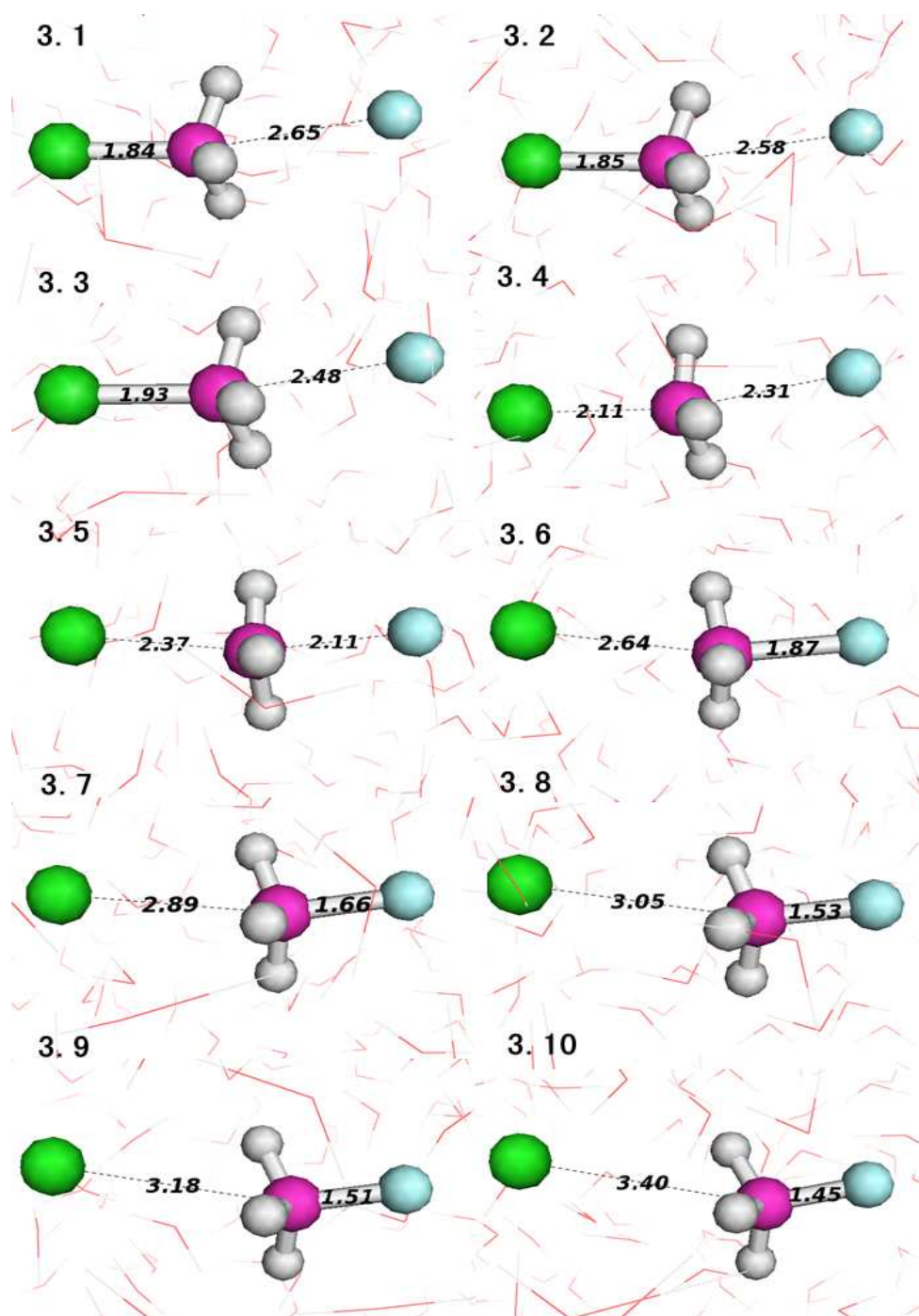
Figure 3. Structures of the ten beads along the NEB reaction pathway for CH_3Cl +

$F^- \rightarrow CH_3F + Cl^-$ in aqueous solution. No. 1 is the structure of the reactant state, No.

5 is the transition state, and No.10 is the product state. The indicated distances are in
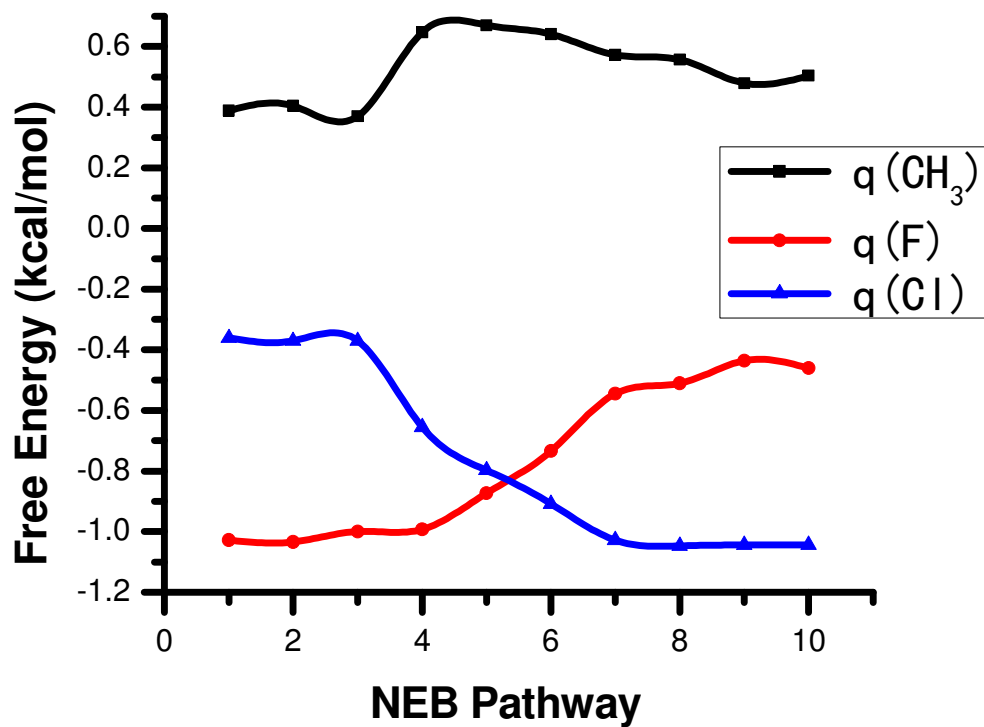
Angstroms.

Figure 4. Charge distributions of the CH$_3$, F and Cl along the NEB reaction pathway

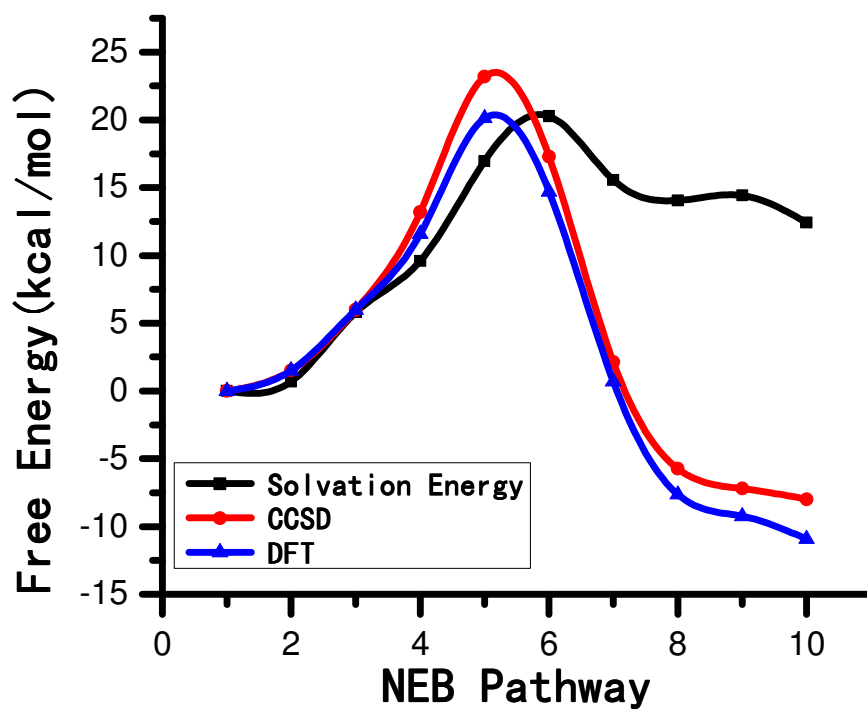for the reaction $CH_3Cl + F^- \rightarrow CH_3F + Cl^-$.

Figure 5. Comparison of the potential of mean force calculated at DFT/MM and CCSD(T)/MM levels of theory and solvation energy contribution using the reactant state (bead 1) as a reference point.
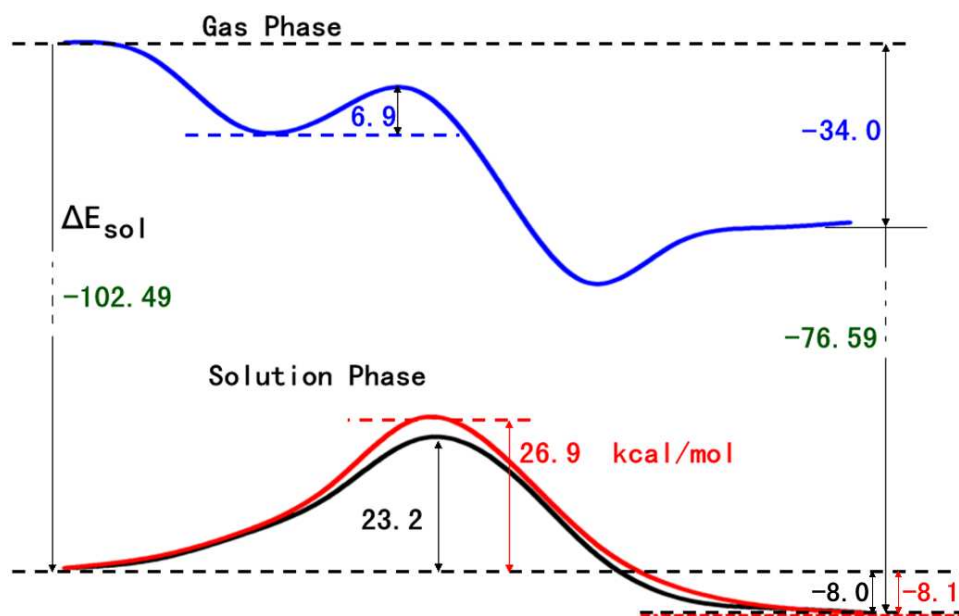
Figure 6. Comparison of schematic free energy profiles in gas phase (blue curve) and

in aqueous solution (Black curve is the PMF calculated under the CCSD(T)/MM level

of theory; red is the estimated one using the gas-phase reaction energy[10] and solvation

energies of the reactant and product,[34,35] the experimental activation barrier height,

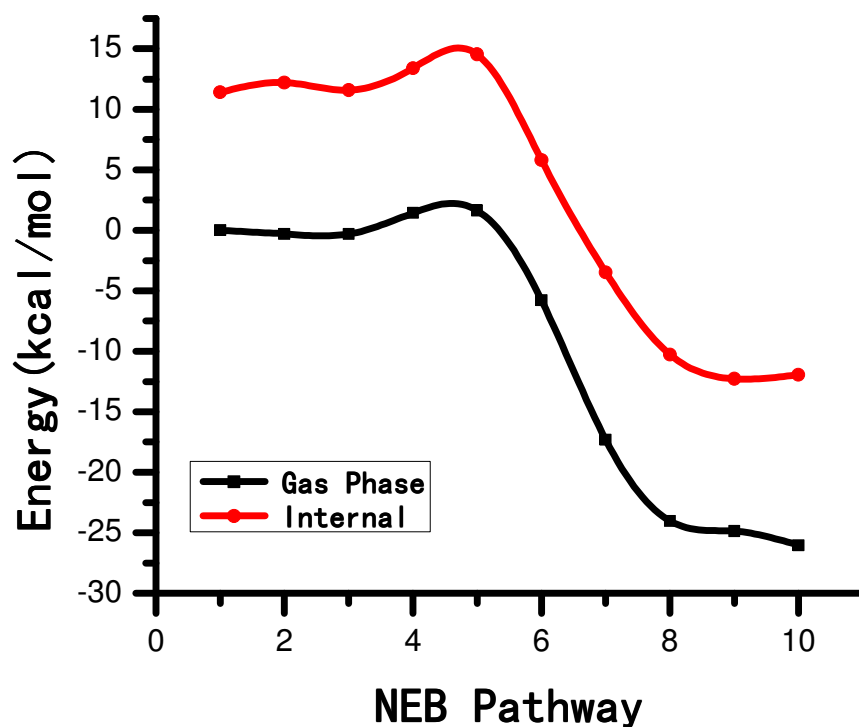26.9 kcal/mol, is taken from Ref. 14).

Figure 7. Comparison between gas-phase and solute internal energies at CCSD(T) level along the NEB reaction pathway using the gas-phase reactant state as a reference point.

22

References

(1) V. K. Gupta, I. Ali, T. A. Saleh, A. Nayak and S. Agarwal, *RSC Adv*. 2012, **2(16)**, 6380.

(2) R. Thiruvenkatachari, S. Vigneswaran and R. Naidu, *J. Ind. Eng. Chem.* 2008, **14(2)**, 145.

(3) U.S. Environmental Protection Agency, Water quality regulatory programs in the Clean Water Act: Toxic and Priority Pollutants, 2013(accessed 11.30.2013). *http://water.epa.gov/scitech/methods/cwa/pollutants.cfm*.

(4) K. Tanaka, G. I. Mackay, J. D. Payzant, and D. K. Bohme, *Can. J. Chem.* 1976, **54**, 1643.

(5) D. K. Bohme and A. B. Raksit, *Can. J. Chem.* 1985, **63**, 3007.

(6) (a) H. Wang and W. L. Hase, *J. Am. Chem. Soc.* 1997, **119**, 3093. (b) T. Su, H. Wang and W. L. Hase, *J. Phys. Chem. A* 1998, **102**, 9819.

(7) W. Hu and D. G. Truhlar, *J. Am. Chem. Soc.* 1994, **116**, 7791.

(8) M. Igarashi and H. Tachikawa, *Int. J. Mass spectrum* 1998, **181**, 151.

(9) H. Tachikawa and M. Igarashi, *Chem. Phys. Lett.* 1999, **303**, 81.

(10) H. Tachikawa, *J. Phys. Chem. A* 2000, **104**, 497.

(11) H. Tachikawa, *J. Phys. Chem. A* 2001, **105**, 1260.

(12) H. Tachikawa, M. Igarashi and T. Ishibashi, *Chem. Phys. Lett.* 2002, **363**, 355.

(13) I. Szabó, A. G. Császár and G. Czakó, *Chem. Sci.*, 2013, **4(12)**, 4362.

(14) R. H. Bathgate and E. A. Moelwyn-Hughes, *J. Chem. Soc.(Resumed)* 1959, 2642.

(15) T. Kozaki, K. Morihashi and O. Kikuchi, *J. Am. Chem. Soc.* 1989, **111**, 1547.

(16) H. Lin and D. G. Truhlar, *Theor. Chem. Acc.* 2007, **117**, 185.

(17) Y. Zhang, H. Liu and W. Yang, *J. Chem. Phys.* 2000, **112**, 3483.

(18) A. Warshel, *Annu. Rev. Biophys. Biomol. Struct.* 2003, **32**, 425.

(19) P. Hohenberg and W. Kohn, *Phys. Rev. B* 1964, **136**, B864.

(20) W. Kohn and L. Sham, *J. Phys. Rev. A* 1965, **140**, A1133.

(21) Y. Zhao, N. González-García and D. G. Truhlar, *J. Phys. Chem. A* 2005, **109(9)**, 2012.

(22) J. F. Stanton and R. J. Bartlett, *J. Chem. Phys.* 1993, **98**, 7029.

(23) R. J. Bartlett and M. Musiał, *Rev. Mod. Phys.* 2007, **79(1)**, 291.

(24) M. Valiev, B. C. Garrett, M. K. Tsai, K. Karol, S. M. Kathmann, G. K. Schenter and M. Dupuis, *J. Phys. Chem.* 2007, **127**, 051102.

(25) D. Wang, M. Valiev and B. C. Garrett, *J. Phys. Chem. A* 2011, **115**, 1380.

(26) M. Valiev, E. J. Bylaska, M. Dupuis and P. G. Tratnyek, *J. Phys. Chem. A* 2008, **112**, 2713.

(27) (a) M. Svensson, S. Humbel, R. D. J. Froese, T. Matsubara, S. Sieber and K. Morokuma, *J. Phys. Chem.*, 1996, **100**, 19357. (b) R. D. J. Froese, K. Morokuma, In The Encyclopedia of Computational Chemistry, P. V. R. Schleyer, N. L. Allinger, T. Clark, J. Gasteiger, P. A. Kollman, H. F. Schaefer III, P. R. Schreiner, Eds., Wiley: Chichester, U.K., 1998. (c) S. Dapprich, I. Komaromi, K. S. Byun, K. Morokuma and M. J. Frisch, *J. Mol. Struct.*, 1999, **462**, 1. (d) P. B. Karadakov and K. Morokuma, *Chem. Phys. Lett.*, 2000, **317**,589. (e) T. Vreven and K. Morokuma, *J. Comput. Chem.*, 2000, **21**, 1419.

(28) T. Vreven, B. Mennucci, C. O. D. Silva, K. Morokuma and J. Tomasi, *J. Chem. Phys.*, 2001, **115**, 62.

(29) M. Cossi, V. Barone, R. Cammi and J. Tomasi, *J. Chem. Phys. Lett.*, 1996, **255**, 327.

(30) A. Klamt and G. Schuurmann, *J. Chem. Soc. Perkin Trans.*, 1993, **5**, 799.

(31) M. Valiev, E. J. Bylaska, N. Govind, K. Kowalski, T. P. Straatsma, D. Wang, J. Nieplocha, E. Apra, T. L. Windus and W. A. deJong, *Comput. Phys. Commun.* 2010, **181**, 1477.

(32) H. J. C. Berendsen, J. R. Grigera and T. P. Straatsma, *J. Phys. Chem.* 1987, **91**, 6269.

(33) J. Zheng, Y. Zhao and D. G. Truhlar, *J. Chem. Theory Comput.*, 2009, **5**, 808.

(34) J. M. Gonzales, R. S. Cox, S. T. Brown, W. D. Allen and H. F. Schaefer, *J. Phys. Chem. A*, 2001, **105**, 11327.

(35) H. Yin, D. Wang and M. Valiev, *J. Phys. Chem. A*, 2011, **115(43)**, 12047.

(36) T. Fox and P. A. Kollman, *J. Phys. Chem. B* 1998, **102**, 8070.

(37) G. Henkelman, B. P. Uberuaga and H. Jónsson, *J. Chem. Phys.* 2000, **113**, 9901.

(38) B. Safi, K. Choho and P. Geerlings, *J. Phys. Chem. A* 2001, **105**, 591.

(39) L. Song, W. Wu, P. C. Hiberty and S. Shaik, *Chem. Eur. J.* 2006, **12**, 7458.

(40) E. J. Bylaska, D. A. Dixon, A. R. Felmy and P. G. Tratnyek, *J. Phys. Chem. A ,*2002, **106**, 11581.
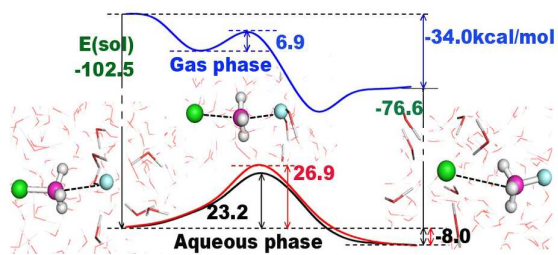
A multi-layered representation, hybrid quantum mechanical and molecular mechanics method study of the $CH_3F + OH^- \rightarrow CH_3OH + F^-$ reaction in water